

# Green Chemistry

Accepted Manuscript



This article can be cited before page numbers have been issued, to do this please use: O. Vozniuk, S. Agnoli, L. Artiglia, A. Vassoï, N. Tanchoux, F. Di Renzo, G. Granozzi and F. Cavani, *Green Chem.*, 2015, DOI: 10.1039/C5GC02139A.



This is an *Accepted Manuscript*, which has been through the Royal Society of Chemistry peer review process and has been accepted for publication.

*Accepted Manuscripts* are published online shortly after acceptance, before technical editing, formatting and proof reading. Using this free service, authors can make their results available to the community, in citable form, before we publish the edited article. We will replace this *Accepted Manuscript* with the edited and formatted *Advance Article* as soon as it is available.

You can find more information about *Accepted Manuscripts* in the [Information for Authors](#).

Please note that technical editing may introduce minor changes to the text and/or graphics, which may alter content. The journal's standard [Terms & Conditions](#) and the [Ethical guidelines](#) still apply. In no event shall the Royal Society of Chemistry be held responsible for any errors or omissions in this *Accepted Manuscript* or any consequences arising from the use of any information it contains.

## Towards an improved process for hydrogen production: the chemical-loop reforming of ethanol

Olena Vozniuk<sup>a</sup>, Stefano Agnoli<sup>b</sup>, Luca Artiglia<sup>b</sup>, Andrea Vassoio<sup>a</sup>, Nathalie Tanchoux<sup>c</sup>, Francesco Di Renzo<sup>c</sup>, Gaetano Granozzi<sup>b,†</sup>, Fabrizio Cavani<sup>a, d, †</sup>

<sup>a</sup> Dipartimento di Chimica Industriale “Toso Montanari”, Università di Bologna, Viale Risorgimento 4, 40136 Bologna, Italy.

<sup>b</sup> Department of Chemical Sciences, Via F. Marzolo 1, 35131 Padova, Italy

<sup>c</sup> Institut Charles Gerhardt Montpellier, ENSCM, 8 Rue Ecole Normale, F-34296 Montpellier, France

<sup>d</sup> INSTM, Research Unit of Bologna, Via G. Giusti 9, Firenze, Italy

† e-mail: [fabrizio.cavani@unibo.it](mailto:fabrizio.cavani@unibo.it); [gaetano.granozzi@unipd.it](mailto:gaetano.granozzi@unipd.it)

Non-stoichiometric M-modified ferros spinels with formula  $M_{0.6}Fe_{2.4}O_x$  (M=Co, Mn or Co/Mn) were employed as ionic oxygen and electron carrier materials for an alternative sustainable route to produce hydrogen via chemical-loop reforming of ethanol. The new materials were tested in terms of both redox properties and catalytic activity to generate hydrogen by oxidation with steam, after a reductive step carried out with ethanol. In addition, the research includes *in-situ* DRIFTS and *in-situ* XPS studies that allowed to extract information at molecular level and to follow surface changes within the reduction/re-oxidation processes during ethanol chemical-loop reforming. It was found that Co(II)-incorporation in spinels effectively improves decomposition/oxidation of ethanol, however a greater amount of coke is accumulated. On the other hand, addition of Mn(II) into the system helps to significantly reduce the amount of coke and hence to avoid a fast deactivation of the material. Thus, the behavior of  $Co_{0.3}Mn_{0.3}Fe_{2.4}O_y$  was shown to be the most promising one, as this material forms less coke during the reduction step, and consequently less  $CO_x$  is generated during the re-oxidation step with water, nevertheless a high hydrogen yield is maintained.

### Introduction

Current processes for the industrial production of hydrogen are based on the reforming of natural gas/naphtha or coal gasification. Such processes are highly energy demanding. Hence, less energy-intensive and more sustainable technologies, exploiting renewable feedstock (such as biomass, bio-

alcohols and water) and renewable primary energy sources (e.g. sunlight, wind, wave or hydro-power), appear to be very attractive for both industry and consumer applications. A variety of new technologies offering a non-fossil based route for hydrogen production are in a different stage of development, and each offers unique opportunities, benefits and challenges.<sup>1–10</sup>

Chemical-loop steam reforming is one of the possible ways to produce H<sub>2</sub> starting from either conventional or renewable sources. Differently from classical reforming, separation costs can be avoided by splitting the process into two alternated steps in order to detach H<sub>2</sub> and CO<sub>x</sub> streams. One of the advantages of this technology relates to its feedstock flexibility. The chemical-loop process can be performed using a number of different reductants, such as gas resulting from coal<sup>11</sup> or biomass<sup>12–14</sup> gasification, light hydrocarbons reforming,<sup>15</sup> methane,<sup>16–18</sup> CH<sub>4</sub>/CO<sub>2</sub> and CH<sub>4</sub>/H<sub>2</sub> mixture,<sup>18,19</sup> pyrolysis oil,<sup>20,21</sup> methanol<sup>22</sup> and pure H<sub>2</sub> (as a method for H<sub>2</sub> storage).<sup>23,24</sup> Furthermore, the nature of the oxide used as the ionic oxygen and electron carrier and the reaction conditions are important parameters since they determine the potential for low costs and high efficiency of this process in order to have a commercial impact. Among the various proposed metal oxides for the chemical-loop approach, the mostly studied ones are pure and mixed iron oxides. Several research groups have been exploring modifications of simple iron oxide (Fe<sub>3</sub>O<sub>4</sub> and Fe<sub>2</sub>O<sub>3</sub>) in order to prevent deactivation,<sup>25</sup> to lower the operating temperature<sup>26</sup> and to increase the structural stability and reducibility,<sup>27,28</sup> the reaction rate for oxidation and total efficiency of the process.<sup>29,30</sup> Several studies were dedicated to different metal additives to iron oxide.<sup>31,32</sup> In addition, ternary metal systems have also been considered in the search for a better synergetic effect.<sup>33,34</sup>

This paper deals with an investigation of spinel type mixed oxides (modified ferros spinels), as the carriers for the production of *clean* hydrogen in the so-called chemical-loop reforming of ethanol (Scheme 1). The choice of ethanol as reducing agent has several advantages: its renewable origin together with the possibility to decompose at a relatively lower temperature with the formation of hydrogen-rich mixture.

In our previous studies,<sup>35–39</sup> we were dealing with stoichiometric binary ferros spinels MFe<sub>2</sub>O<sub>4</sub> (M = Fe, Co, Ni or Cu), as carrier materials, which have shown promising features for hydrogen production. The initial experiments were carried out with methanol as reducing agent. According to the obtained results we concluded that the morphology of the CoFe<sub>2</sub>O<sub>4</sub> spinel (calcined at 450 and 750°C) led to differences in methanol anaerobic decomposition and oxidation; however, after a first complete cycle, the sintering effect resulted in a strong modification of these properties.<sup>35</sup> In addition, a complete re-oxidation of CoFe<sub>2</sub>O<sub>4</sub> to its original oxidation state was not possible using only water as the oxidant; thus a third step, with the partial re-oxidation of the material with air was needed for a completion of the cycle.<sup>36</sup> The sintering phenomena of magnetite<sup>37</sup> and reaction

mechanism<sup>38</sup> together with deactivation phenomena<sup>39</sup> of methanol and ethanol anaerobic decomposition/oxidation over mixed ferros spinels were also investigated.

The present work is focused on new non-stoichiometric binary and ternary M-modified ferros spinels (i.e. mixed solid solutions) for the chemical-loop reforming of bio-ethanol that can operate in mild temperature range for both reduction and re-oxidation steps. Substitution of Fe centers with other transition metals leads to the formation of an inverse, normal, or mixed spinels with different degree of inversion. Besides this, such an introduction may strongly modify the redox properties of the resultant ferros spinels.<sup>40</sup>

Several research groups have investigated the effect of various M-additives on the stability and redox behavior of iron oxide for chemical hydrogen storage using, amongst others, Pd, Pt, Rh, Ru, Al, Ce, Ti, Zr<sup>41</sup> and Al, Cr, Zr, Ga, V, Mo<sup>42</sup>. For example it was found out that Pd, Pt, Rh and Ru additives have an effect of promoting the reduction and lowering the re-oxidation temperature of iron oxide. At the same time, Al, Ce, Ti, Zr, Cr, Ga and V additives prevent deactivation and sintering of iron oxide during repeated redox cycles. However, according to our knowledge, a systematic study on the role of dopants and their effect on the chemical-physical properties of the resulting mixed M-modified ferrites as future perspective materials for chemical-loop reforming of ethanol has not been done until now. Thus, the aim of this work is to investigate the behavior of these new materials in the two-step chemical-loop reforming of bio-ethanol. Particularly the focus is on the reactivity behavior of ternary materials based on Co-Mn ferros spinels with different Co:Mn atomic ratios. The special interest in the Co and/or Mn doping is explained by their ability to form thermodynamically stable spinel oxides which allowed us to both re-obtain the initial spinel phase upon cycling and increase the stability of the looping material.

## Experimental

### Materials preparation

M-modified non-stoichiometric ferros spinels with different Co:Mn atomic ratio (where Co:Mn = 1:0; 0.9:0.1; 0.5:0.5 and 0:1) and nominal composition  $M^{1}_{0.6-x}M^2_xFe_{2.4}O_y$  were prepared by the co-precipitation method. Nitrate precursors were used for all of the synthesized materials. The mixed solutions of metal precursors containing 100mL of 1M  $Fe(NO_3)_3 \cdot 9H_2O$ , 50mL of 0.5M  $M(NO_3)_2 \cdot xH_2O$  (or 50mL of 0.25M  $M^1(NO_3)_2 \cdot xH_2O$  and  $M^2(NO_3)_2 \cdot xH_2O$ ) were put into a separation funnel and then drop-by-drop added into the reaction vessel containing 0.5L of 2M NaOH aqueous solution at the temperature of 50°C under vigorous stirring with a constant speed. The suspensions were stirred for 2h at the constant temperature of 50°C adding NaOH 3M in order to maintain the pH above 13. The precipitates were separated by vacuum filtration by means of a Büchner funnel

and then washed with about 1.5L of distilled water at room temperature (RT), to remove sodium and nitrates ions. The washed samples were dried at 120°C in air for 12 h, milled in agate mortar and then calcined in static air at 450°C for 8h with the heating rate of 10°C/min.

### Materials characterization

The specific surface area was measured, applying the single-point BET method. The instrument used was a Carlo Erba Sorptly 1700. For the analysis, around an amount of 0.5 g of the sample was placed inside the sample holder and then heated at 150°C under vacuum (2 MPa) to release water, air, CO<sub>2</sub> or other molecules adsorbed. Subsequently the sample was placed in liquid nitrogen, and the adsorption of the gaseous N<sub>2</sub> was carried out.

For TEM/EDX characterisation, samples were suspended in ethanol and homogenized using ultrasonication (for 5 min). The suspension was deposited on a holey-carbon film Cu-grid for TEM analysis, then dried at 100°C. The analyses were carried out by a microscope TEM/ STEM FEI TECNAI F20 at 200 keV.

The instrument used for Thermal-Programmed-Reduction (TPR) experiments was the TPR 1100 analyzer from Thermo Quest. The samples were first pre-treated at 450°C for 45 min in He flow (30 mL/min). Reduction (TPR) was carried out with 5 % H<sub>2</sub> in the Ar flow (30 mL/min). Temperature program started at 50°C and then the temperature was increased up to 800°C (with ramp 10°C/min) and maintained for 40 min.

Raman spectra were recorded using a Bruker spectrometer with a 633 nm He/Ne laser source (filter: P<sub>laser</sub> ÷10; slit 100 µm) equipped with a microscope (50X lens). Each spectrum was taken with 300 sec exposure time and 1 accumulation.

The powder X-ray diffraction (XRD) patterns were measured on Bruker D8 Advance diffractometer (using Cu K<sub>α</sub> radiation at  $\lambda = 1.5418 \text{ \AA}$ ) with a Bragg-Brentano geometry and equipped with a Bruker Lynx Eye detector. The data were recorded from 5 to 80° 2 $\theta$  diffraction angle with an acquisition time of 1 s per each step.

Diffuse-Reflectance Infrared FT spectroscopy, coupled with a quadrupole mass spectrometer (DRIFTS-MS) was used to characterise the surface features of materials. During a standard procedure, the sample was pre-treated at 450°C in a He flow (5mL/min) for 1 h in order to remove molecules possibly adsorbed on the material, mainly carbon dioxide and water. Then the sample was cooled down to 30°C, and the IR background was collected. Afterward ethanol was fed at 0.6 mL/min until saturation was reached (as seen by IR and MS; around 20 min) and whereupon the He flow was maintained until the weakly adsorbed ethanol was evacuated from the cell with loaded catalyst. During evacuation, the DRIFT and mass spectra were taken to follow stabilization of the

system. When the mass and DRIFT spectra were stable, the temperature was increased up to 150°C for 2 min and then the system was cooled down to 30°C to record the spectra. This last step was repeated for the other temperatures (150, 200, 250, 300, 350 and 400°C).<sup>38</sup>

X-ray photoemission spectroscopy (XPS) data were acquired using non-monochromatized Al K $\alpha$  (1486.6 eV) X-ray source, and an Omicron EA125 electron analyser. The measurements were carried out in a custom built ultra-high-vacuum system operating at the base pressure of  $5 \times 10^{-10}$  mbar equipped with facilities for sample heating and controlled gas dosing. The spectra were acquired at RT on drop casted films of powder samples suspended in water. Different sample treatments have been carried out: annealing in UHV at 450°C, reduction with ethanol at 450°C ( $5 \times 10^{-6}$  mbar) and re-oxidation at 450°C in water ambient ( $2 \times 10^{-4}$  mbar). For each of four M-modified ferros spinels Fe 2*p*, O1*s* and Co 2*p* and/or Mn 2*p* photoemission spectra were recorded sequentially after introduction in the UHV systems (“as received”), after annealing in UHV for 30 min at 450°C, after exposure to ethanol at 450°C and after H<sub>2</sub>O exposure at 450°C.

### Reactivity tests of ethanol chemical-loop reforming

Reactivity experiments were carried out by loading 400 mg of the pelletized sample (with particles diameter  $\approx 0.25$  to 0.6 mm), in the fixed-bed quartz flow reactor with an internal diameter of 12mm and a length of 30 cm; the catalytic bed height was less than 2 mm. The reduction reaction was carried out by feeding continuously a stream of ethanol vapors (15.6 mol%) in N<sub>2</sub>; the latter was also used as a standard; contact time was 0.25 s. For the re-oxidation step, water steam (29.3 mol%) was fed in a N<sub>2</sub> flow. Reactivity experiments were carried out at different cycling conditions with chosen duration of the reduction/re-oxidation steps (20 min red·1cyc/20 min ox·1cyc). The reaction temperature for both steps was 450°C. The products were monitored on-line by an Agilent 3000A micro-GC with 3 parallel columns: (a) a PlotQ column, with He carrier, for the separation of CH<sub>4</sub>, CO<sub>2</sub>, H<sub>2</sub>O and ethanol; (b) a OV1 column, with He carrier, for the separation of CO<sub>2</sub>, acetaldehyde, H<sub>2</sub>O, ethanol; (c) a Molecular Sieve 5A column, Ar carrier, for the separation of H<sub>2</sub>, O<sub>2</sub>, N<sub>2</sub>, CH<sub>4</sub>, and CO. A Plot U backflash column was installed in order to avoid CO<sub>2</sub> and H<sub>2</sub>O poisoning in the third column. Yields of each product were calculated by the same method as described in detail in Ref. <sup>39</sup>.

## Results and discussion

### *Bulk samples characterization*

XRD patterns of the calcined materials at 450°C (for 8 h) are shown in Figure 1. All M-modified non-stoichiometric ferros spinels display a spinel phase of magnetite (Fe<sub>3</sub>O<sub>4</sub>), as reported in our

previous papers,<sup>37,36</sup> even though Mn-based samples exhibit a lower crystallinity or are partially in amorphous form. Table 1 reports the surface area measurements. The highest surface area is shown by  $\text{Mn}_{0.6}\text{Fe}_{2.4}\text{O}_y$ , and this value declines with an increase of Co-content, which may be explained by a decrease of the particle size in Mn-modified samples. Moreover, the particle size, morphology and structure of the samples were investigated by means of TEM. The results indicate that the samples prepared by co-precipitation method are almost uniform in both morphology and particle size distribution (~2-6 nm) (Figure 2-A).

Table 1. Specific surface area for calcined samples

Sample	Surface area, $\text{m}^2/\text{g}$
$\text{Co}_{0.6}\text{Fe}_{2.4}\text{O}_y$	$74 \pm 2$
$\text{Co}_{0.54}\text{Mn}_{0.06}\text{Fe}_{2.4}\text{O}_y$	$88 \pm 2$
$\text{Co}_{0.3}\text{Mn}_{0.3}\text{Fe}_{2.4}\text{O}_y$	$138 \pm 3$
$\text{Mn}_{0.6}\text{Fe}_{2.4}\text{O}_y$	$157 \pm 3$

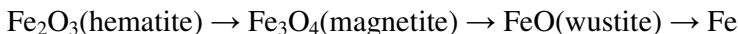
Several  $\text{MFe}_2\text{O}_4$  ferros spinels exhibit inversion of the cations between the tetrahedral and octahedral sites. Normally,  $\text{Fe}_3\text{O}_4$  and  $\text{CoFe}_2\text{O}_4$  are completely inverse spinels; however, unlike the other ferros spinels,  $\text{MnFe}_2\text{O}_4$  is a normal spinel.<sup>43</sup> In spite of this, nanostructured powders of various synthesis and treatment methods can exhibit different degrees of inversion. In order to disclose the information on the internal structure, i.e. bonding and distribution of substituted ions among the octahedral (Oh) and tetrahedral (Td) sites of the materials, Raman Spectroscopy measurements were performed. Raman features of ferros spinels are highly specific, i.e. they are depending on stoichiometry, cation distribution, defects, and also on the experimental conditions.<sup>44</sup> Spectra of the inverse spinels are more complicated and show additional Raman-active modes over the five Raman modes predicted by group theory:  ${}^{44}\text{F}_{2g}(1)$ ,  $\text{E}_g$ ,  $\text{F}_{2g}(2)$ ,  $\text{F}_{2g}(3)$  and  $\text{A}_{1g}$ . Additional modes may appear in vibrational spectra due to local distortions of the crystal lattice. These defects do not affect the long-range ordering of the system, and often cannot be detected by XRD.

Figure 3 shows the Raman spectra of the calcined materials. The spectrum A -  $\text{Co}_{0.6}\text{Fe}_{2.4}\text{O}_y$  reveals 6 vibration modes: 5 predicted by the literature and an additional one caused by the local distortions in the lattice. The five first order Raman modes are at about 182, 300, 471, 554 and  $688 \text{ cm}^{-1}$ . The most intense vibration mode at  $688 \text{ cm}^{-1}$  is the  $\text{A}_{1g}$ , which can be assigned to the  $\text{AO}_4$  stretching, and for the inverse ferros spinels it should be the same for all the samples since the  $\text{Fe}^{3+}$  cations are occupying these Td sites. However, with an increase of the Mn-content the shape and the position

of the  $A_{1g}$  at  $688\text{ cm}^{-1}$ , which corresponds to the Fe-O symmetric stretching in Td sites, changes. The band shifts to a lower frequency at about  $657\text{ cm}^{-1}$  and becomes broader (Figure 3-B,C). The other four modes are decreasing in intensity and for  $\text{Mn}_{0.6}\text{Fe}_{2.4}\text{O}_y$  sample, they vanish completely.  $\text{Mn}^{2+}$  ions are proposed to partially replace  $\text{Fe}^{3+}$  ions in the Td sites (partly due to the non-stoichiometric composition of the ferros spinels), which may cause the change of the inversion degree towards the formation of the normal spinel.<sup>43</sup> The resulting spectrum of  $\text{Mn}_{0.6}\text{Fe}_{2.4}\text{O}_y$  is in agreement with previous reports.<sup>45</sup> The low intensity of the peaks and partial energy shifts can be related also to a high defectivity<sup>46</sup> and a low crystallinity as confirmed by XRD.

TPR measurements were performed in order to investigate the role of different metals on reducibility of samples. The position of the temperature maxima may vary from sample to sample depending on the particle size and other parameters such as temperature ramp rate. The substitution of ferrous iron with another  $\text{M}^{2+}$  ion affects the oxygen mobility in the solid, thus modifies the reducibility of the material.<sup>47</sup> In Figure 4, the deconvolution of reduction profiles was based on reduction steps and corresponding temperature maxima, as inferred from the literature.<sup>40,47–49</sup>

All M-modified non-stoichiometric ferros spinels show mainly two steps of the reduction processes: the reduction of iron oxide to metallic iron and the reduction of the other metal oxide to metal. The reduction of iron oxide:



strongly depends on the presence of another metal oxide in M-modified ferros spinels.<sup>47,48</sup> In the TPR profile of  $\text{Co}_{0.6}\text{Fe}_{2.4}\text{O}_y$  (Figure 4-A), the reduction of hematite to magnetite is observed at  $\sim 400^\circ\text{C}$ , followed by the reduction of  $\text{Co}_3\text{O}_4$  to  $\text{CoO}$  at  $\sim 502^\circ\text{C}$  and of  $\text{CoO}$  to metallic  $\text{Co}$  at  $\sim 576^\circ\text{C}$ , and finally magnetite to wustite reductive transition was observed at  $\sim 690^\circ\text{C}$ . Further reduction of wustite to metallic  $\text{Fe}^0$  appears around  $780^\circ\text{C}$ , but the complete reduction of the  $\text{FeO}$  to  $\text{Fe}^0$  could not be observed.

Following the TPR profile of  $\text{Mn}_{0.6}\text{Fe}_{2.4}\text{O}_y$  (Figure 4-D), the first peak at  $200^\circ\text{C}$  corresponds to the reduction of  $\text{Mn}^{4+}$  to  $\text{Mn}^{3+}$ , while the reduction of  $\text{Mn}^{3+}$  to  $\text{Mn}^{2+}$  occurs at  $525^\circ\text{C}$ . It turned out that it is difficult for  $\text{MnO}$  to be further reduced to  $\text{Mn}^0$ , due to its highly negative reduction potential ( $-1.18\text{ eV}$ ), thus there was no evidence of the  $\text{MnO}$  reduction process under the present experimental conditions. The  $616^\circ\text{C}$  peak corresponds to the reduction of magnetite to wustite, beyond which total reduction to metallic iron is expected to occur. These results are in a good agreement with the report of Khan et al.<sup>48</sup> The presence of Mn facilitates the reduction of  $\text{Fe}^{3+}$  species [ $\text{Fe}_2\text{O}_3$  to  $\text{Fe}_3\text{O}_4$ ]. However, the reduction of  $\text{FeO} \rightarrow \text{Fe}^0$  appears at higher temperature,  $\sim 850^\circ\text{C}$ , than for the other M-modified non-stoichiometric ferros spinels. This effect could be primarily attributed to the formation of either normal or mixed spinels of composition  $A_\delta B_{(1-\delta)}[A_\delta B_{(2-\delta)}]O_4$ .

In the case of Co/Mn-modified ferrosin systems (Figure 4-B,C)  $\text{Fe}_2\text{O}_3 \rightarrow \text{Fe}_3\text{O}_4$  reduction appears at  $\sim 400^\circ\text{C}$ ,  $\text{Fe}_3\text{O}_4 \rightarrow \text{FeO}$  at  $\sim 700^\circ\text{C}$  and  $\text{FeO} \rightarrow \text{Fe}^0$  at  $\sim 800^\circ\text{C}$ . For the reduction of other metals we found:  $\text{Co}_x\text{O}_y$  to  $\text{Co}^0$  ( $\text{Co}_3\text{O}_4 \rightarrow \text{CoO}$  at  $\sim 500^\circ\text{C}$ ,  $\text{CoO} \rightarrow \text{Co}$  at  $\sim 600^\circ\text{C}$ ) and  $\text{Mn}_x\text{O}_y$  to  $\text{MnO}$  ( $\text{Mn}^{4+} \rightarrow \text{Mn}^{3+}$  at  $\sim 200^\circ\text{C}$ ,  $\text{Mn}^{3+} \rightarrow \text{Mn}^{2+}$  at  $\sim 560^\circ\text{C}$ ). In particular, Co/Mn systems present a cooperative influence of both Mn and Co on each other's reduction profiles (Table S1).

Therefore, from TPR measurements it can be concluded that incorporation of different metal cations into magnetite structure alters its reducibility, which in turn is affected by the nature of the incorporated metal cation. However, it is also important to evaluate the reducibility of the materials using ethanol as reducing agent. The information about the ethanol adsorption and its further transformation into different intermediate species was obtained using *in-situ* DRIFTS study.

### **Surface characterization: DRIFT spectroscopy**

The adsorption of alcohols over metal oxides can lead to different kind of adsorbed species depending on the surface properties of the material under study. According to the literature, ethanol adsorbs on the surface mainly as an ethoxide, formed from the scission of the O-H bond.<sup>50-54</sup> However, the species formed with increasing temperatures are more related to the surface chemistry of each compound.<sup>38</sup> Figure 5 shows spectra of adsorbed ethanol at RT over the four samples. Ethoxy bands (dissociative adsorption) can be observed at  $1057$  and  $1103\text{ cm}^{-1}$  for the C-O/C-C stretching modes together with the bands of the undissociated ethanol (at  $1383\text{ cm}^{-1}$  and  $1274\text{ cm}^{-1}$  for  $\text{CH}_3\delta$  and  $\text{OH}\delta$ , respectively).<sup>38,55</sup> The complex absorption in the  $2800\text{-}2400\text{ cm}^{-1}$  region is probably due to a Fermi resonance of the overtone of the  $\text{OH}\delta$  vibration mode with the CH-stretching modes at  $2971$ ,  $2929$ , and  $2863\text{ cm}^{-1}$  ( $\text{CH}_3(\text{as})$ ,  $\text{CH}_2(\text{as})$  and  $\text{CH}_3(\text{s})$  modes of the ethoxide species).<sup>52,38</sup> Figures 5(A-C) show a strong band at  $3252\text{ cm}^{-1}$  that may be assigned to the OH stretching of ethanol H-bonded to the surface, which also was observed over the stoichiometric  $\text{CoFe}_2\text{O}_4$  ferrosin in our previous paper.<sup>38</sup> The sharp band at  $3681\text{ cm}^{-1}$  together with a shoulder at  $3635\text{ cm}^{-1}$  is assigned to the  $-\text{OH}$  stretching vibration of chemisorbed undissociated ethanol over surface Lewis acid sites ( $\text{M}^{n+}$ ).<sup>56-58</sup> The shoulder at lower frequency may indicate the presence of different active sites on the materials. However, with increasing the Mn-content the shoulder decreases in intensity and only for  $\text{Mn}_{0.6}\text{Fe}_{2.4}\text{O}_y$  it completely disappears. This effect was already seen by Raman spectroscopic, described above.

Some remarkable differences between the DRIFTS spectra of samples are observed when the temperature is increased (Figure 6); acetate bands appear (at  $1334$ ,  $1439$ ,  $1590\text{ cm}^{-1}$  for the  $\text{CH}_3\delta$ ,  $\text{OCOv}(\text{s})$ , and  $\text{OCOv}(\text{as})$  vibrations, respectively). The increasing in intensity and broadening of the band at  $1590\text{ cm}^{-1}$  (at  $250^\circ\text{C}$ ) also indicates the formation of carbonate species.<sup>59</sup> These species

could further produce CO<sub>2</sub>, which is detected as the doublet at the 2358-2338 cm<sup>-1</sup> region and corresponds to adsorbed and/or gaseous CO<sub>2</sub> rotation vibration P and R bands.<sup>60</sup> The DRIFT spectra obtained on Mn<sub>0.6</sub>Fe<sub>2.4</sub>O<sub>4</sub> (Fig 6-D), also exhibit the bands for acetate species, formed by the reaction of ethoxy species with surface oxygen (1598, 1555, 1433 and 1334 cm<sup>-1</sup>).<sup>53,61</sup> When the temperature is increased (up to 400°C) the intensity of the bands corresponding to ethoxy species is reduced, whereas the bands associated with acetate species (strongly bounded to the surface) remain almost unchanged. However, the main difference between the spectra of Mn<sub>0.6</sub>Fe<sub>2.4</sub>O<sub>4</sub> and of other Co- and Co-Mn ferrosinels spectra lies in the absence of the bands associated with carbonate species; the band of the adsorbed CO<sub>2</sub> was not observed as well. Thus, the results may indicate that Co and Co-Mn-modified systems were more reactive than the Mn ferrosinels. This is also followed by the presence of a broad absorbed feature in the 3000-1800 cm<sup>-1</sup> region, which is attributed to the electronic absorption of the partially reduced sample.<sup>38,62</sup>

In summary, the redox properties of M-modified ferrosinels and hence their catalytic activity in the chemical-loop reforming of ethanol (see below) are strongly influenced by the nature of M and by the M<sup>n+</sup> distribution among the Oh and Td sites in the crystal lattice. The main differences between the four non-stoichiometric spinels studied are the following: the incorporation of only Co leads to the formation mainly of an inverse spinel, however the addition of Mn resulted in the substitution of Td coordinated Fe<sup>3+</sup> ions with Mn<sup>2+</sup> and as a consequence the formation of new type of active sites. The reduction of M-modified ferrosinels appears to be a complex process due to the presence of various reduced forms of Fe oxides together with oxides of substituted metal ions (Co<sub>x</sub>O<sub>y</sub> and Mn<sub>x</sub>O<sub>y</sub>). Besides, it was observed that incorporation of Co-Mn metal cations into magnetite structure affects its reducibility, which directly depends on the nature of the incorporated metal cation. In particular, the Co-Mn system presents a cooperative influence on each other's reduction profiles. Moreover, during the ethanol anaerobic decomposition/oxidation step over Co and mixed Co-Mn ferrosinels, acetates and carbonates appeared to be important surface intermediates and in the case of the only Mn containing catalyst, there was no evidence for the carbonates formation.

#### ***Surface characterization: photoemission spectroscopy***

In order to study the kinetics of the reduction and re-oxidation processes that take place on the catalytic surface, *in-situ* XPS measurements were performed. In particular, by monitoring the changes occurred in the photoemission spectra of Fe2p, Co2p and Mn2p, during ethanol (5×10<sup>-6</sup> mbar at 450°C) and water (2×10<sup>-4</sup> mbar at 450°C) exposure, it was possible to determine the role played by each component of the Co/Mn-modified ferrosinels on the surface chemistry.

Let us first concentrate on the changes in the XPS data after the sample annealing at 450°C in UHV. As an example, in Figure S1 we compare the spectra of  $\text{Co}_{0.3}\text{Mn}_{0.3}\text{Fe}_{2.4}\text{O}_y$  as received and after annealing: a significant decrease of the FWHM in the  $\text{O}1s$  spectrum and a small shift of  $\text{Fe}2p$  and  $\text{Mn}2p$  peaks lower binding energy (BE) values are clearly observed, which indicate a surface modification occurred after elimination of the adsorbed hydroxyl ( $\text{OH}^-$ ) groups or/and water molecules, and the reduction of highly oxidized metal species (e.g.  $\text{Fe}_2\text{O}_3$  to  $\text{Fe}_3\text{O}_4$  formation). In any case, the spectra obtained after this UHV annealing are taken as a reference for the subsequent chemical changes induced by the chemical treatments.

The chemical composition determined by photoemission and the spectral fingerprints observed confirm the presence of M-modified ferros spinels whose stoichiometric ratio is in agreement with the nominal ratio of the synthesis protocol.

The samples were exposed to an increasing amount of ethanol and the evolution of the main core level spectra (see Figures S2, S3, S4, S5), was measured observing clear differences in the surface composition as a function of the presence of different M.

Starting from the very beginning of ethanol feeding, the reduction of iron from  $\text{Fe}^{3+}$  to  $\text{Fe}^{2+}$  was observed for all tested samples, which is evidenced by the decrease of the intensity of the  $\text{Fe}2p$  peak in conjunction with the energy shift of  $\text{Fe}2p_{3/2}$  satellite from 8 eV (typical for  $\text{Fe}^{3+}$ ) to 5 eV, which can be ascribed to oxides with a lower valence.<sup>63,64</sup>

In the case of prolonged ethanol exposure, the appearance of a further component at 707.0 eV indicates the formation of a metal component. Such a phenomenon is strongly dependent on the actual composition of the corresponding sample, and especially on the Co:Mn ratio. As shown in Figure 7, it was found that Co(II)-incorporation effectively improves the reducibility of the catalyst, whereas addition of Mn has an opposite effect. This effect is once again confirmed by the previously described TPR and DRIFTS results. Moreover,  $\text{Co}_{0.54}\text{Mn}_{0.06}\text{Fe}_{2.4}\text{O}_y$  showed a stronger reduction in comparison to the sample without Mn ( $\text{Co}_{0.6}\text{Fe}_{2.4}\text{O}_y$  - Figure 7). This behaviour can be explained by the size effect induced by the presence of Mn (with increasing of Mn-content the specific surface area also increased). In the  $\text{Co}_{0.3}\text{Mn}_{0.3}\text{Fe}_{2.4}\text{O}_y$  ferros spinel within 80 min of reduction by ethanol, a peak corresponding to the formation of an iron metal phase was not detected and it was seen only after 120 min of ethanol feeding (see Figure S3). This resilience towards the reduction was observed also for  $\text{Mn}_{0.6}\text{Fe}_{2.4}\text{O}_y$ , whose reduction behaviour is very similar (see Figure S2).

Moreover, we could observe changes in the line shape of  $\text{Mn}2p$  only after the annealing in UHV at 450°C (due to the desorption of surface  $\text{OH}^-$  groups and/or water molecules), whereas afterwards spectra remained unchanged, despite the iron and cobalt underwent substantial reduction.

It has been already mentioned that Co boosts the reduction of ferros spinels; however it is interesting to compare the tendency toward the reduction of Co vs Fe. The photoemission peak of Co2p overlaps with Fe Auger peak, which complicates its analysis, nevertheless some qualitative information can be obtained. Cobalt is present as Co<sup>2+</sup> and therefore no more reduced species can be formed, but the metal. As a matter of fact in the Co2p photoemission line it can be observed a progressive disappearance of the Co<sup>2+</sup> 2p<sub>1/2</sub> peaks (795.5 eV) and its satellite in favour of the formation of a metal component (793.3 eV). Metal components of Fe and Co were observed almost at the same time, however it can be noted that cobalt was fully reduced to metal in the case Co<sub>0.6</sub>Fe<sub>2.4</sub>O<sub>y</sub> and Co<sub>0.54</sub>Mn<sub>0.06</sub>Fe<sub>2.4</sub>O<sub>y</sub> whereas the reduction of iron species to metallic iron was only partial (Figure 7).

In the case of relatively large Mn-content (Co<sub>0.3</sub>Mn<sub>0.3</sub>Fe<sub>2.4</sub>O<sub>y</sub>), Co cations are not reduced immediately, but a relevant oxidized component can be observed in standard conditions (80 min of ethanol feeding), whereas only after 120 min is fully reduced. It is also interesting to note that such reaction seems to be autocatalytic; actually in the stage from 80 to 120 min there is a fast increase in the reduced components with the formation of metallic phases. These experiments suggest that when Mn is present in large amount there is a substantial depression of reduction. This indicates that the synthesized ferros spinel are homogeneous and not a physical mixture of Co<sub>0.6</sub>Fe<sub>2.4</sub>O<sub>y</sub> and Mn<sub>0.6</sub>Fe<sub>2.4</sub>O<sub>y</sub>. Moreover, the chemical activity of the M-modified ferros spinels is ruled in a complex way by the sum of the effects due to the two incorporated metals.

To summarize the picture emerging from the XPS investigation we can propose that the reduction process involves the fast formation of a reduced oxide with a satellite at 5 eV and afterwards the nucleation of iron metal. This shift of the satellite can be qualitatively associated with the reduction of Fe<sup>3+</sup> to Fe<sup>2+</sup> which from the structural point of view corresponds to the reduction to wustite, and only afterwards this latter is progressively reduced to metal iron.

The formation of the metal phase seems to be a rather slow process and requires a significant induction period whereas the first reduction from Fe<sup>3+</sup> to Fe<sup>2+</sup> is quite fast in the used conditions.

Globally from photoemission we can outline a *scenario* where the reactivity of the ferros spinels is strongly dependent on the type of M introduced in the lattice, which however determines a quite complex reactivity scheme based on a synergetic effect. Manganese in large amount has the effect of slowing down the reduction reaction and in any case it can never be reduced. The high thermodynamic stability of Mn<sup>2+</sup> is the probable origin of its scarce attitude toward reduction. Cobalt on the contrary can be reduced to the metallic state very quickly, even faster and in a larger extent than iron.

In order to get information on the second step of the chemical loop we have investigated the exposure of ethanol reduced  $\text{Co}_{0.6}\text{Fe}_{2.4}\text{O}_y$  and  $\text{Co}_{0.3}\text{Mn}_{0.3}\text{Fe}_{2.4}\text{O}_y$  to water at  $450^\circ\text{C}$  (see Figures S3 and S5). In both cases  $\text{Fe}2p$  spectra indicate a fast oxidation process that leads to an almost complete suppression of the metal component. However it must be noted that the final  $\text{Fe}2p$  spectrum is rather broad with a smeared fine structure, which can be due to the co-presence of many different phases: not only ferros spinels but also iron suboxides and hydroxides. The presence of these latter is supported by the larger FWHM and increased intensity on the high BE side of the O 1s peak after water dosing. Similarly in the  $\text{Co}2p$  spectra, the quick formation of oxidized species i.e.  $\text{Co}^{2+}$  can be observed immediately after water exposure. However, whereas in the pure cobalt ferros spinel the oxidation of cobalt is almost quantitative, in the case of the Co/Mn sample such process is partial and a large metal cobalt component is visible even after extended water dosing (60 min). Such difference can be probably traced back to the presence of manganese, which somehow hinders the reaction with water.

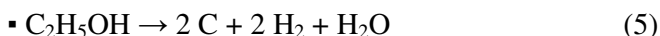
### Reactivity tests

Figure 8 shows conversion and yield for the main products (yield >5%), obtained during the first step of the chemical loop, where the material is being reduced by ethanol at  $450^\circ\text{C}$  for 20 min. The cycling time was chosen according to the initial results achieved over pristine  $\text{Fe}_3\text{O}_4$  and stoichiometric ferros spinels -  $\text{CoFe}_2\text{O}_4$ ,  $\text{NiFe}_2\text{O}_4$ <sup>37,39</sup>. We reported that in approximately 20 min of ethanol feeding, the material was constantly reduced until it reached its 'steady state' with the stable composition under these reaction conditions. Therefore, we were able to avoid a further coke deposition that occurred over the strongly reduced spinel.

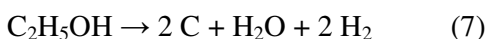
The conversion of ethanol over  $\text{Co}_{0.6}\text{Fe}_{2.4}\text{O}_y$  (Figure 8-A) reached 100% starting from the first minutes of the reaction, and it was stable during 20 min of ethanol feeding. One of the main products of ethanol conversion was hydrogen, with an initial yield of about 50%, which increased up to 82% while the extent of spinel reduction increased. Also, CO and  $\text{CO}_2$  showed similar increasing trends as for  $\text{H}_2$ , thus suggesting that the main reactions during spinel reduction involved the partial oxidation of ethanol:



The formation of acetone, which declined with time, can be a result of an aldol condensation of the intermediately formed acetaldehyde, with further isomerization of aldol into hydroxyketone followed by a reverse reaction to form acetone and formaldehyde (converted into CO and  $\text{H}_2$ ). The formation of water (with yield ~11%) involves several possible reactions:



Coke and heavy compounds (mainly aromatics) also formed starting from the very beginning of the reaction time (~20%), with a progressive increase in yield. Under these reaction conditions it was impossible to avoid the formation of carbonaceous species. The generation of coke was likely due to dehydrogenation and total deoxygenation of ethanol:



Moreover, disproportionation of CO (Boudouard reaction) can result in coke deposition:



Results obtained with the other samples (Figures 8–B,C,D) demonstrate similar trends in the products distribution. However, some significant differences can be seen: with increasing Mn-content the conversion of ethanol was slightly decreasing. The  $\text{Mn}_{0.6}\text{Fe}_{2.4}\text{O}_y$  sample (Figure 8-D) at first showed 100% of conversion followed by its decrease down to 80%. The main reason for such behavior can be an accumulation of MnO phase in the catalyst, which has a high thermodynamic stability and as a consequence its scarce attitude towards the reduction to metallic component. This result also has been confirmed by TPR, DRIFTS and in-situ XPS measurements.

As discussed above, we could not completely avoid coke formation, but despite this, we were able to significantly reduce its amount by changing the composition of the catalyst, as shown in Figure 9, plotting the overall yield to C residues integrated over the 20 min reduction time. Indeed, the presence of Mn had the beneficial effect of decreasing the coke deposition, which is an important issue in order to produce C-free hydrogen. The integrated yields for other products formed during 20 min of reduction with ethanol are plotted in Figure S6. In particular, Co-containing ferros spinels ( $\text{Co}_{0.6}\text{Fe}_{2.4}\text{O}_y$  and  $\text{Co}_{0.54}\text{Mn}_{0.06}\text{Fe}_{2.4}\text{O}_y$ ) have shown high yields to  $\text{CO}_2$ , CO and  $\text{H}_2\text{O}$  and enhanced reactivity in the anaerobic decomposition/oxidation of ethanol. On the other hand,  $\text{Mn}_{0.6}\text{Fe}_{2.4}\text{O}_y$  appeared to be more active in the formation of acetone, which is the result of the reverse aldol condensation reaction.

Figure S7 shows the degree of reduction for the four catalysts with different ratio Co/Mn as a function of reaction time (20 min), as calculated from the oxygen balance<sup>39</sup>. Even though the highest surface area was shown by  $\text{Mn}_{0.6}\text{Fe}_{2.4}\text{O}_4$  catalyst, and it declined with an increase of Co-content, the samples with high content of Co ( $\text{Co}_{0.6}\text{Fe}_{2.4}\text{O}_y$  and  $\text{Co}_{0.54}\text{Mn}_{0.06}\text{Fe}_{2.4}\text{O}_y$ ) were strongly reduced (almost 100 %) in comparison to only Mn-modified ferros spinel with just ca 20% of reduction extent. This suggests that the difference in the reducibility of the four M-modified

ferrospinel is related to the nature of the incorporated M cation and its intrinsic reactivity, which is also confirmed by in-situ XPS results.

After the reduction with ethanol, the materials were re-oxidized with steam at 450°C, which corresponds to the second step of the chemical loop. Figure S8(A-D) reports the yield of H<sub>2</sub>, CO<sub>2</sub> and CO versus time (yields have been calculated based on the H or O content in products, with respect to the water fed), whereas Figure 10 reports the overall yields to H<sub>2</sub>, CO and CO<sub>2</sub>, integrated over the 20 min oxidation time. High hydrogen yields were obtained over Co<sub>0.6</sub>Fe<sub>2.4</sub>O<sub>y</sub>, Co<sub>0.54</sub>Mn<sub>0.06</sub>Fe<sub>2.4</sub>O<sub>y</sub> and Co<sub>0.3</sub>Mn<sub>0.3</sub>Fe<sub>2.4</sub>O<sub>y</sub>. The common problem of all samples was the formation of CO and CO<sub>2</sub> during the re-oxidation step (Figs.10 and S8), because of the gasification of carbonaceous residues, previously formed during the reduction step. The main difference was in the amount of produced CO<sub>x</sub>. According to the obtained results, Mn-containing catalysts were more selective to hydrogen formation, as shown in Table 2, reporting the ratio between the overall yield to H<sub>2</sub> and the overall yield to CO+CO<sub>2</sub>.

In order to quantify the real amount of coke formed on the tested materials an elemental analysis (CHNS) was carried out. Table 3 shows the obtained results: Mn-containing materials (Mn<sub>0.6</sub>Fe<sub>2.4</sub>O<sub>y</sub> and Co<sub>0.3</sub>Mn<sub>0.3</sub>Fe<sub>2.4</sub>O<sub>y</sub>) showed the lowest amount of C residues accumulated during the first reduction step. However, with all materials a part of the coke still remained on the surface after one complete cycle, being not completely re-oxidized with water at that temperature (450°C). As a consequence, these materials underwent some morphological changes significantly affected by accumulation of coke, sintering (particle size increased to ~90-100 nm) and segregation (see Figures 2-B,C; these images are of samples which underwent several redox cycles).

However, the behavior shown by Co<sub>0.3</sub>Mn<sub>0.3</sub>Fe<sub>2.4</sub>O<sub>y</sub> can be considered the most promising one, since it forms less coke during the 1<sup>st</sup> step of ethanol reduction and less CO<sub>x</sub> during the 2<sup>nd</sup> step of re-oxidation with steam, nevertheless it can provide high hydrogen yield. On the other hand, Mn<sub>0.6</sub>Fe<sub>2.4</sub>O<sub>y</sub> and Mn<sub>0.3</sub>Co<sub>0.3</sub>Fe<sub>2.4</sub>O<sub>y</sub> were less efficient in the removal of C residues during the re-oxidation with steam; this means that the low amount of CO and CO<sub>2</sub> formed during the 2<sup>nd</sup> step are also due to the fact that coke is only in minimal part re-oxidised by steam. This may be due to the lower degree of reduction achieved during the 1<sup>st</sup> step, since the reduced metal may catalyze the gasification of coke by reaction with steam. As already pointed out, a third step of re-oxidation with air is necessary in order to completely remove the C residues formed during the reduction with ethanol.<sup>22,65</sup>

Table 2. Ratio  $H_2/(CO+CO_2)$  obtained during the re-oxidation step with water

	$H_2/CO+CO_2$
$Mn_{0.6}Fe_{2.4}O_y$	28.0
$Mn_{0.3}Co_{0.3}Fe_{2.4}O_y$	12.2
$Mn_{0.06}Co_{0.54}Fe_{2.4}O_y$	5.2
$Co_{0.6}Fe_{2.4}O_y$	5.0

Table 3. Amount of coke (C) in weight % obtained over the four samples investigated

	C content(%) after 20 min of reduction (ethanol)	C content(%) after 20 min reduction (ethanol) + 20 min re-oxidation ( $H_2O$ )
$Mn_{0.6}Fe_{2.4}O_y$	2.2	2.1
$Co_{0.3}Mn_{0.3}Fe_{2.4}O_y$	7.9	6.5
$Co_{0.54}Mn_{0.06}Fe_{2.4}O_y$	11.0	6.1
$Co_{0.6}Fe_{2.4}O_y$	9.7	6.2

## Conclusions

The chemical-loop reforming of ethanol for  $H_2$  production was studied by using M-modified non-stoichiometric ferros spinels as ionic oxygen carrier materials. The redox properties of ferros spinels were found to depend strongly on the nature of incorporated cation in addition to its distribution inside the crystal lattice. The four catalysts with different ratio between two supplemented metals (Co/Mn) were investigated. Substitution of  $Fe^{2+}$  with  $Co^{2+}$  ions led to the formation mainly of an inverse spinel, however the addition of Mn resulted in the substitution of Td coordinated  $Fe^{3+}$  ions with  $Mn^{2+}$  and as a consequence the formation of new type of active sites. The reduction of M-modified ferros spinels appeared to be a complex process due to the presence of various reduced forms of Fe oxides together with Co and Mn oxides. Besides, it was observed that incorporation of Mn-Co metal cations into magnetite ( $Fe_3O_4$ ) crystal structure affects its reducibility, depending on the nature of the incorporated metal cation. In particular, Co/Mn systems showed a cooperative influence on each other's reduction profiles. Moreover, in-situ DRIFTS study was performed in order to follow the stepwise reduction of the catalyst surface, which allowed us to detect different adsorbed species and their transformation into the products. Acetates and carbonates appeared to be important surface intermediates over Co- and mixed Co-Mn ferros spinels and in the case of the only Mn-containing catalyst, there was no evidence of the carbonates formation. Furthermore, according

to the results obtained by means of catalytic tests and CHNS elemental analysis, the addition of Mn hindered carbon deposition, which also caused a decrease of the amount of  $\text{CO}_x$  generated by oxidation with water steam, which is an important issue to produce clean  $\text{H}_2$ . However, the Mn containing ferros spinels showed a lower efficiency in the removal of the C residues accumulated during the first step. This may lead to the need of a third step of coke removal by air oxidation, if a clean material is needed to perform a following cycle. In an alternative approach, as already pointed out in the literature, the unreactive coke may be maintained as an inert material, provided (that) during successive cycles the further accumulation of coke occurs at a limited extent only<sup>22,65</sup>.

Co-Mn mixed ferros spinels, with high levels of Co, enhanced reactivity in the anaerobic decomposition/oxidation of ethanol. Thus, the behavior shown by  $\text{Co}_{0.3}\text{Mn}_{0.3}\text{Fe}_{2.4}\text{O}_y$  can be considered to be the most promising one, as this type of M-modified ferros spinel formed less coke during the reduction step (as a result less  $\text{CO}_x$  generated during the re-oxidation step with water), and still high hydrogen yield could be obtained.

Therefore, one of the key points to improve the proposed process and make it industrially attractive is reducing the amount of carbonaceous species which in principle can be done by changing the catalyst composition and thus tuning its redox properties in order to optimize the ratio between the degree of reduction and the amount of coke deposition.

Hence, the use of bulk M-modified spinel oxides as oxygen carrier materials for the chemical-loop reforming of ethanol shows a positive aspect which allows to achieve a good recyclability of the starting material due to the formation of thermodynamically stable spinel oxide phase during cycling, using the same mild temperatures for both reduction and re-oxidation steps. This may be an advantage compared to other approaches reported in literature, such as the use of high temperatures<sup>66,67</sup> to limit coke formation and structured materials with morphologies aimed to confine the negative effects of sintering<sup>68-70</sup>.

### Acknowledgements

The EU is acknowledged for the grant to OV (SINCHEM, The European Doctoral Program on Sustainable Industrial Chemistry). We thank Mr. L. Calore (University of Padova) for the CHNS elemental analyses. This work has been also funded by the Italian Ministry of Instruction, University and Research (MIUR) through the FIRB Project RBAP115AYN Oxides at the nanoscale: multifunctionality and applications.

**Figures captions**

Scheme 1. The chemical-loop reforming of ethanol over modified ferros spinels

Figure 1. XRD patterns of ferrites calcined at 450°C: (A)  $\text{Co}_{0.6}\text{Fe}_{2.4}\text{O}_y$ ; (B)  $\text{Co}_{0.54}\text{Mn}_{0.06}\text{Fe}_{2.4}\text{O}_y$ ; (C)  $\text{Co}_{0.3}\text{Mn}_{0.3}\text{Fe}_{2.4}\text{O}_y$ ; (D)  $\text{Mn}_{0.6}\text{Fe}_{2.4}\text{O}_y$

Figure 2. TEM images of  $\text{Co}_{0.3}\text{Mn}_{0.3}\text{Fe}_{2.4}\text{O}_y$ : (A) fresh material calcined at 450°C; (B) after 4 cycles • 20 min + 1 red • 20 min; (C) after 20 min • 5 cycles

Figure 3. Raman spectra of the ferrites calcined at 450°C: (A)  $\text{Co}_{0.6}\text{Fe}_{2.4}\text{O}_y$ ; (B)  $\text{Co}_{0.54}\text{Mn}_{0.06}\text{Fe}_{2.4}\text{O}_y$ ; (C)  $\text{Co}_{0.3}\text{Mn}_{0.3}\text{Fe}_{2.4}\text{O}_y$ ; (D)  $\text{Mn}_{0.6}\text{Fe}_{2.4}\text{O}_y$

Figure 4. TPR profile Co/Mn-modified non-stoichiometric ferros spinels. (A)  $\text{Co}_{0.6}\text{Fe}_{2.4}\text{O}_y$ ; (B)  $\text{Co}_{0.54}\text{Mn}_{0.06}\text{Fe}_{2.4}\text{O}_y$ ; (C)  $\text{Co}_{0.3}\text{Mn}_{0.3}\text{Fe}_{2.4}\text{O}_y$ ; (D)  $\text{Mn}_{0.6}\text{Fe}_{2.4}\text{O}_y$

Figure 5. DRIFTS spectra after adsorption of ethanol at 30°C: (A)  $\text{Co}_{0.6}\text{Fe}_{2.4}\text{O}_y$ , (B)  $\text{Co}_{0.54}\text{Mn}_{0.06}\text{Fe}_{2.4}\text{O}_y$ , (C)  $\text{Co}_{0.3}\text{Mn}_{0.3}\text{Fe}_{2.4}\text{O}_y$ , (D)  $\text{Mn}_{0.6}\text{Fe}_{2.4}\text{O}_y$

Figure 6. DRIFTS spectra recorded at increasing temperatures: (A)  $\text{Co}_{0.6}\text{Fe}_{2.4}\text{O}_y$ , (B)  $\text{Co}_{0.54}\text{Mn}_{0.06}\text{Fe}_{2.4}\text{O}_y$ , (C)  $\text{Co}_{0.3}\text{Mn}_{0.3}\text{Fe}_{2.4}\text{O}_y$ , (D)  $\text{Mn}_{0.6}\text{Fe}_{2.4}\text{O}_y$ .

Figure 7: (top) Fe 2p and (bottom) Co 2p photoemission spectra after the exposure to ethanol at 450°C for 80 minutes

Figure 8. Conversion and yields for the main products during 20 min reduction with ethanol at 450°C over: (A)  $\text{Co}_{0.6}\text{Fe}_{2.4}\text{O}_y$ ; (B)  $\text{Co}_{0.54}\text{Mn}_{0.06}\text{Fe}_{2.4}\text{O}_y$ ; (C)  $\text{Co}_{0.3}\text{Mn}_{0.3}\text{Fe}_{2.4}\text{O}_y$ ; (D)  $\text{Mn}_{0.6}\text{Fe}_{2.4}\text{O}_y$ .

Figure 9. Integrated Yields for the coke and heavy compounds during 20 min reduction with ethanol at 450°C.

Figure 10. Integrated values of yields to  $\text{H}_2$ ,  $\text{CO}_2$  and CO during the re-oxidation with  $\text{H}_2\text{O}$ .

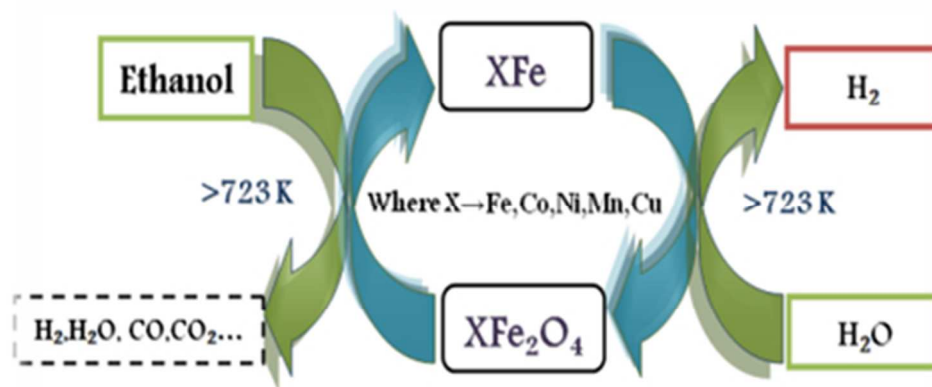
## References

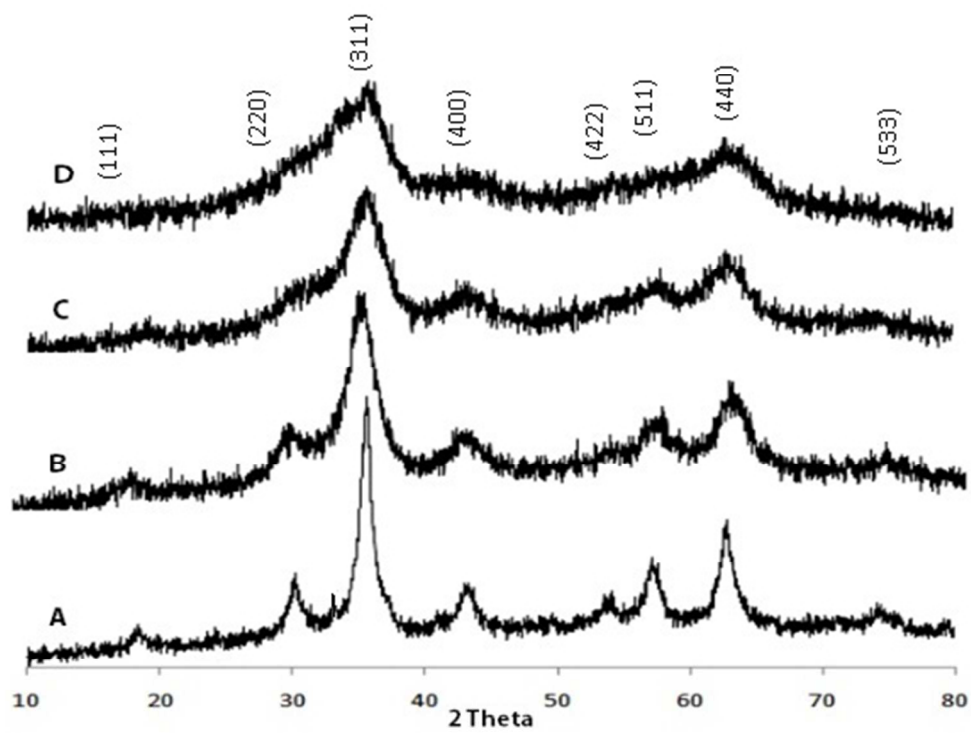
- 1 R. M. Navarro, M. C. Sánchez-Sánchez, M. C. Alvarez-Galvan, F. Del Valle and J. L. G. Fierro, *Energy Environ. Sci.*, 2009, **2**, 35–54.
- 2 G. Tsekouras, D. Neagu and J. T. S. Irvine, *Energy Environ. Sci.*, 2013, **6**, 256–266.
- 3 B. K. Boggs, R. L. King and G. G. Botte, *Chem. Commun. (Camb)*., 2009, 4859–4861.
- 4 T. Lazarides, M. Delor, I. V. Sazanovich, T. M. McCormick, I. Georgakaki, G. Charalambidis, J. A. Weinstein and A. G. Coutsolelos, *Chem. Commun. (Camb)*., 2014, **50**, 521–523.
- 5 J. W. Jurss, R. S. Khnayer, J. A. Panetier, K. A. El Roz, E. M. Nichols, M. Head-Gordon, J. R. Long, F. N. Castellano and C. J. Chang, *Chem. Sci.*, 2015, **6**, 4954–4972.
- 6 M. Ni, D. Y. C. Leung and M. K. H. Leung, *Int. J. Hydrogen Energy*, 2007, **32**, 3238–3247.
- 7 L. Chen, C. K. S. Choong, Z. Zhong, L. Huang, T. P. Ang, L. Hong and J. Lin, *J. Catal.*, 2010, **276**, 197–200.
- 8 F. Fresno, T. Yoshida, N. Gokon, R. Fernández-Saavedra and T. Kodama, *Int. J. Hydrogen Energy*, 2010, **35**, 8503–8510.
- 9 P. Charvin, S. Abanades, G. Flamant and F. Lemort, *Energy*, 2007, **32**, 1124–1133.
- 10 N. Hanada, S. Hino, T. Ichikawa, H. Suzuki, K. Takai and Y. Kojima, *Chem. Commun. (Camb)*., 2010, **46**, 7775–7.
- 11 P. Gupta, L. G. Velazquez-Vargas and L. Fan, *Energy and Fuels*, 2007, **21**, 2900–2908.
- 12 V. Hacker, R. Fankhauser, G. Faleschini, H. Fuchs, K. Friedrich, M. Muhr and K. Kordes, *J. Power Sources*, 2000, **86**, 531–535.
- 13 V. Hacker, G. Faleschini, H. Fuchs, R. Fankhauser, G. Simader, M. Ghaemi, B. Spreitz and K. Friedrich, *J. Power Sources*, 1998, **71**, 226–230.
- 14 R. Sime, J. Kuehni, L. D. Souza, E. Elizondo and S. Biollaz, 2003, **28**, 491–498.
- 15 V. Hacker, *J. Power Sources*, 2003, **118**, 311–314.
- 16 K. Go, S. Son, S. Kim, K. Kang and C. Park, *Int. J. Hydrogen Energy*, 2009, **34**, 1301–1309.
- 17 K. Go, S. Son and S. Kim, *Int. J. Hydrogen Energy*, 2008, **33**, 5986–5995.
- 18 K. Otsuka, A. Mito, S. Takenaka and I. Yamanaka, 2001, **26**, 191–194.
- 19 V. V. Galvita, H. Poelman and G. B. Marin, *Top. Catal.*, 2011, **54**, 907–913.
- 20 M. Bleeker, S. Gorter, S. Kersten, L. van der Ham, H. van den Berg and H. Veringa, *Clean Technol. Environ. Policy*, 2009, **12**, 125–135.
- 21 M. F. Bleeker, S. R. a. Kersten and H. J. Veringa, *Catal. Today*, 2007, **127**, 278–290.

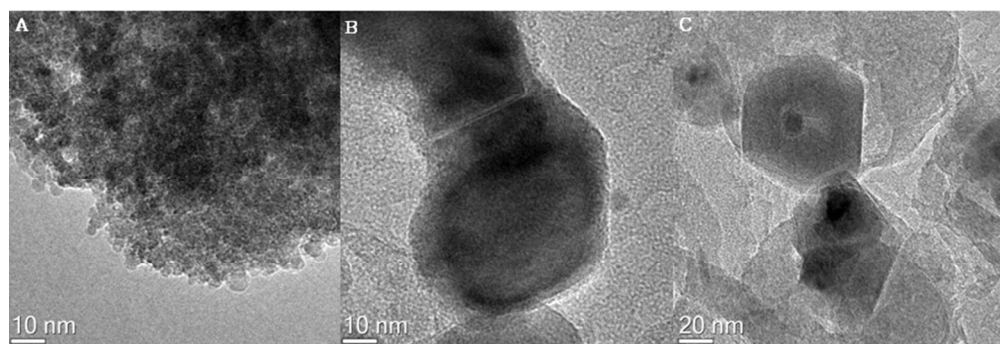
- 22 R. Campo, P. Durán, J. Plou, J. Herguido and J. a. Peña, *J. Power Sources*, 2013, **242**, 520–526.
- 23 J. A. Peña, E. Lorente, E. Romero and J. Herguido, *Catal. Today*, 2006, **116**, 439–444.
- 24 E. Lorente, J. A. Peña and J. Herguido, *J. Power Sources*, 2009, **192**, 224–229.
- 25 K.-S. Cha, H.-S. Kim, B.-K. Yoo, Y.-S. Lee, K.-S. Kang, C.-S. Park and Y.-H. Kim, *Int. J. Hydrogen Energy*, 2009, **34**, 1801–1808.
- 26 K.-S. Kang, C.-H. Kim, W.-C. Cho, K.-K. Bae, S.-W. Woo and C.-S. Park, *Int. J. Hydrogen Energy*, 2008, **33**, 4560–4568.
- 27 D. Yamaguchi, L. Tang, L. Wong, N. Burke, D. Trimm, K. Nguyen and K. Chiang, *Int. J. Hydrogen Energy*, 2011, **36**, 6646–6656.
- 28 S. Takenaka, N. Hanaizumi, V. Son and K. Otsuka, *J. Catal.*, 2004, **228**, 405–416.
- 29 K.-S. Kang, C.-H. Kim, K.-K. Bae, W.-C. Cho, W.-J. Kim, Y.-H. Kim, S.-H. Kim and C.-S. Park, *Int. J. Hydrogen Energy*, 2010, **35**, 568–576.
- 30 T. Kodama, T. Shimizu, T. Satoh and M. Nakata, 2003, **73**, 363–374.
- 31 K. Otsuka, T. Kaburagi, C. Yamada and S. Takenaka, *J. Power Sources*, 2003, **122**, 111–121.
- 32 E. Lorente, J. a. Peña and J. Herguido, *Int. J. Hydrogen Energy*, 2011, **36**, 7043–7050.
- 33 S. Takenaka, T. Kaburagi, C. Yamada, K. Nomura and K. Otsuka, *J. Catal.*, 2004, **228**, 66–74.
- 34 S. Takenaka, K. Nomura, N. Hanaizumi and K. Otsuka, *Appl. Catal. A Gen.*, 2005, **282**, 333–341.
- 35 V. Crocella, F. Cavani, G. Cerrato, S. Cocchi, M. Comito, G. Magnacca and C. Morterra, *J. Phys. Chem. C*, 2012, **116**, 14998–15009.
- 36 S. Cocchi, M. Mari, F. Cavani and J.-M. M. Millet, *Appl. Catal. B Environ.*, 2014, **152-153**, 250–261.
- 37 C. Trevisanut, F. Bosselet, F. Cavani and J. M. M. Millet, *Catal. Sci. Technol.*, 2015, **5**, 1280–1289.
- 38 J. V. Ochoa, C. Trevisanut, J.-M. M. Millet, G. Busca and F. Cavani, *J. Phys. Chem. C*, 2013, **117**, 23908–23918.
- 39 C. Trevisanut, M. Mari, J.-M. M. Millet and F. Cavani, *Int. J. Hydrogen Energy*, 2015, **40**, 5264–5271.
- 40 A. Khan, P. Chen, P. Boolchand and P. Smirniotis, *J. Catal.*, 2008, **253**, 91–104.
- 41 J. C. Ryu, D. H. Lee, K. S. Kang, C. S. Park, J. W. Kim and Y. H. Kim, *J. Ind. Eng. Chem.*, 2008, **14**, 252–260.

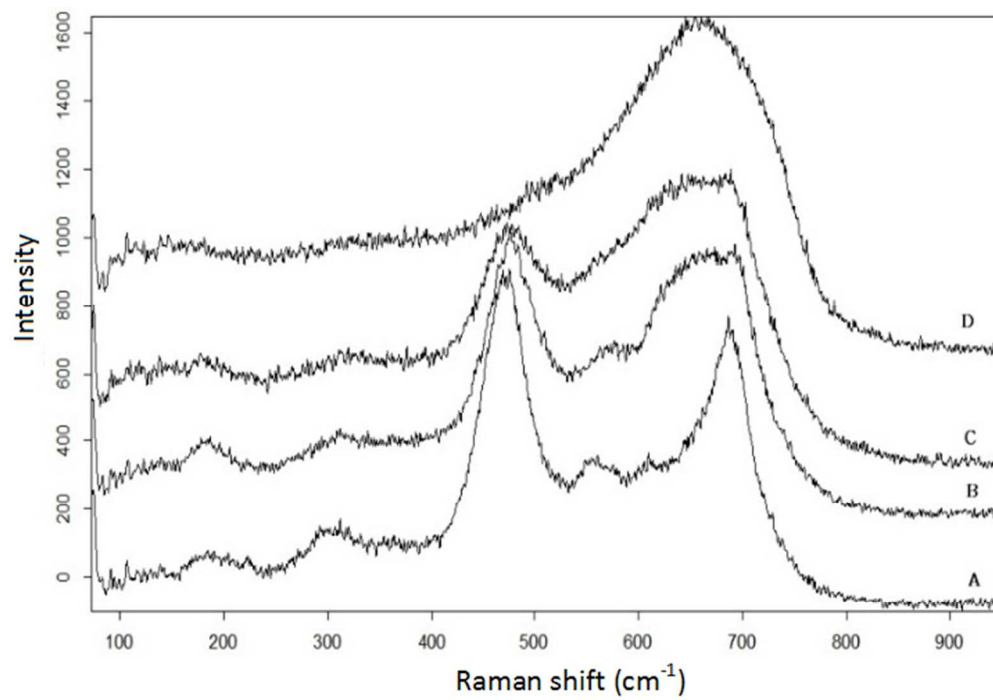
- 42 K. Otsuka, C. Yamada, T. Kaburagi and S. Takenaka, *Int. J. Hydrogen Energy*, 2003, **28**, 335–342.
- 43 N. Z. Lazarevic, Z. Jovalekic, C. Milutinovic, A. Romcevic, M.J. Romcevic, *Acta Phys. Pol. A*, 2012, **121**, 682–686.
- 44 C. S. S. R. Kumar, Ed., *Raman Spectroscopy for Nanomaterials Characterization*, Springer Berlin Heidelberg, Berlin, Heidelberg, 2012.
- 45 J. J. Graves, P.R., Johnston, C., Campaniello, *Mater. Res. Bull.*, 1988, **23**, 1651–1660.
- 46 P. Chandramohan, M. P. Srinivasan, S. Velmurugan and S. V. Narasimhan, *J. Solid State Chem.*, 2011, **184**, 89–96.
- 47 G. K. Reddy, P. Boolchand and P. G. Smirniotis, *J. Phys. Chem. C*, 2012, **116**, 11019–11031.
- 48 A. Khan and P. G. Smirniotis, *J. Mol. Catal. A Chem.*, 2008, **280**, 43–51.
- 49 L. Zhang and Y. Wu, *Hindawi Publ. Corp. J. Nanomater.*, **2013**, 6.
- 50 C. Resini, T. Montanari, L. Barattini, G. Ramis, G. Busca, S. Presto, P. Riani, R. Marazza, M. Sisani, F. Marmottini and U. Costantino, *Appl. Catal. A Gen.*, 2009, **355**, 83–93.
- 51 S. S. Ata-Allah, *J. Magn. Magn. Mater.*, 2004, **284**, 227–238.
- 52 M. Domok, M. Toth, J. Rasko and a Erdohelyi, *Appl. Catal. B Environ.*, 2007, **69**, 262–272.
- 53 K. Rintramee, K. Föttinger, G. Rupprechter and J. Wittayakun, *Appl. Catal. B Environ.*, 2012, **115-116**, 225–235.
- 54 G. Busca, U. Costantino, T. Montanari, G. Ramis, C. Resini and M. Sisani, *Int. J. Hydrogen Energy*, 2010, **35**, 5356–5366.
- 55 M. Schmal, D. V. Cesar, M. M. V. M. Souza and C. E. Guarido, *Can. J. Chem. Eng.*, 2011, **89**, 1166–1175.
- 56 T. W. Birky, J. T. Kozlowski and R. J. Davis, *J. Catal.*, 2013, **298**, 130–137.
- 57 T. Mathew, B. B. Tope, N. R. Shiju, S. G. Hegde, B. S. Rao and C. S. Gopinath, *Phys. Chem. Chem. Phys.*, 2002.
- 58 G. Busca, *Phys. Chem. Chem. Phys.*, 1999, **1**, 723–736.
- 59 L. Mattos and F. Noronha, *J. Catal.*, 2005, **233**, 453–463.
- 60 A. Boudjemaa, C. Daniel, C. Mirodatos, M. Trari, A. Auroux and R. Bouarab, *Comptes Rendus Chim.*, 2011, **14**, 534–538.
- 61 L. V. Mattos and F. B. Noronha, *J. Power Sources*, 2005, **152**, 50–59.
- 62 G. Busca, *Catal. Today*, 1996, **27**, 457–496.
- 63 M. C. Biesinger, B. P. Payne, A. P. Grosvenor, L. W. M. Lau, A. R. Gerson and R. S. C. Smart, *Appl. Surf. Sci.*, 2011, **257**, 2717–2730.

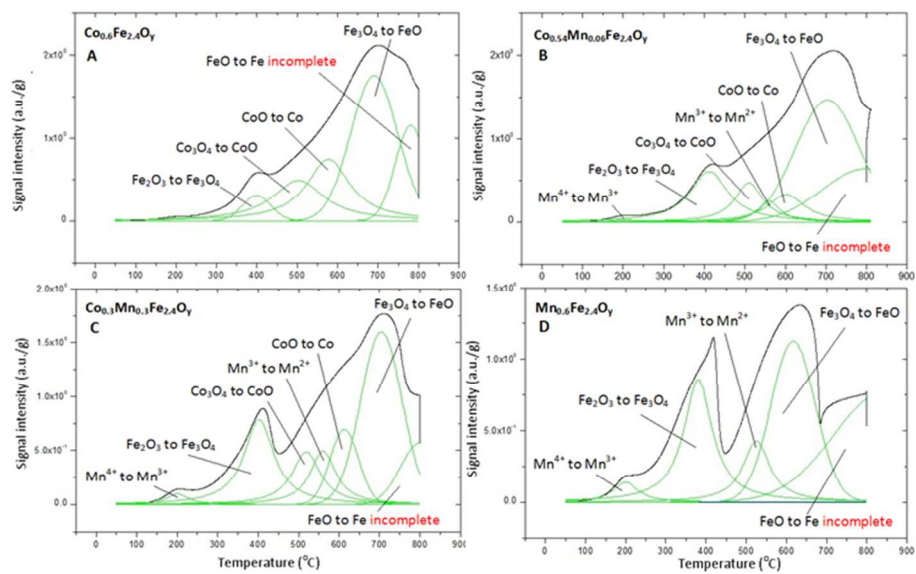
- 64 A. P. Grosvenor, B. A. Kobe, M. C. Biesinger and N. S. McIntyre, *Surf. Interface Anal.*, 2004, **36**, 1564–1574.
- 65 E. Hormilleja, P. Durán, J. Plou, J. Herguido and J. a. Peña, *Int. J. Hydrogen Energy*, 2014, **39**, 5267–5273.
- 66 J. R. Scheffe, M. D. Allendorf, E. N. Coker, B. W. Jacobs, A. H. McDaniel and A. W. Weimer, *Chem. Mater.*, 2011, **23**, 2030–2038.
- 67 K. S. Kang, C. H. Kim, K. K. Bae, W. C. Cho, S. H. Kim and C. S. Park, *Int. J. Hydrogen Energy*, 2010, **35**, 12246–12254.
- 68 L. Neal, A. Shafieifarhood and F. Li, *Appl. Energy*, 2015.
- 69 B. M. Corbella, L. F. De Diego, F. García-Labiano, J. Adánez and J. M. Palacios, *Energy & Fuels*, 2005, **19**, 433–441.
- 70 Z. Sarshar, Z. Sun, D. Zhao and S. Kaliaguine, *Energy & Fuels*, 2012, **26**, 3091–3102.

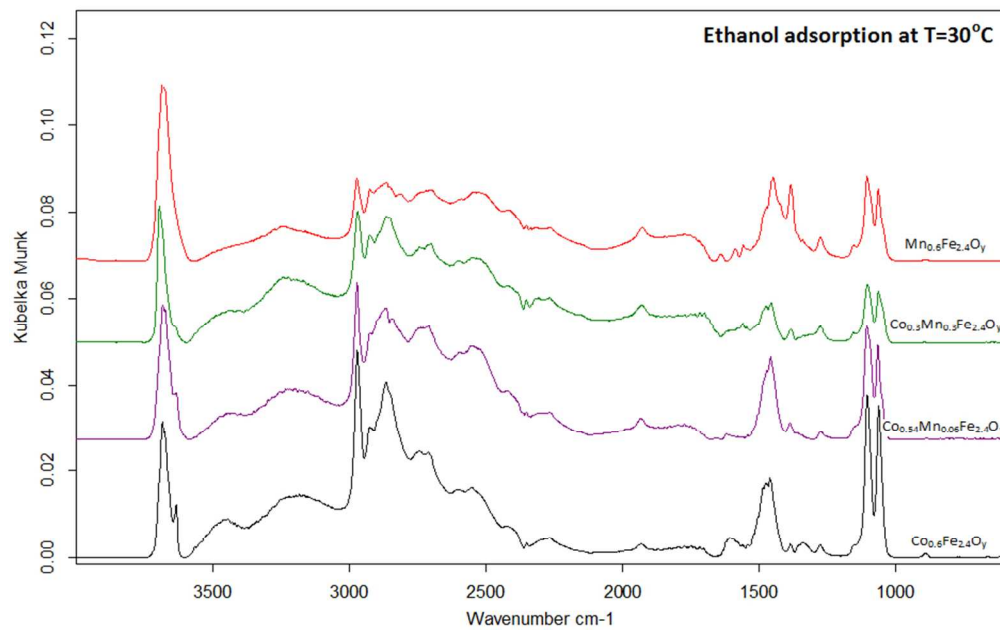


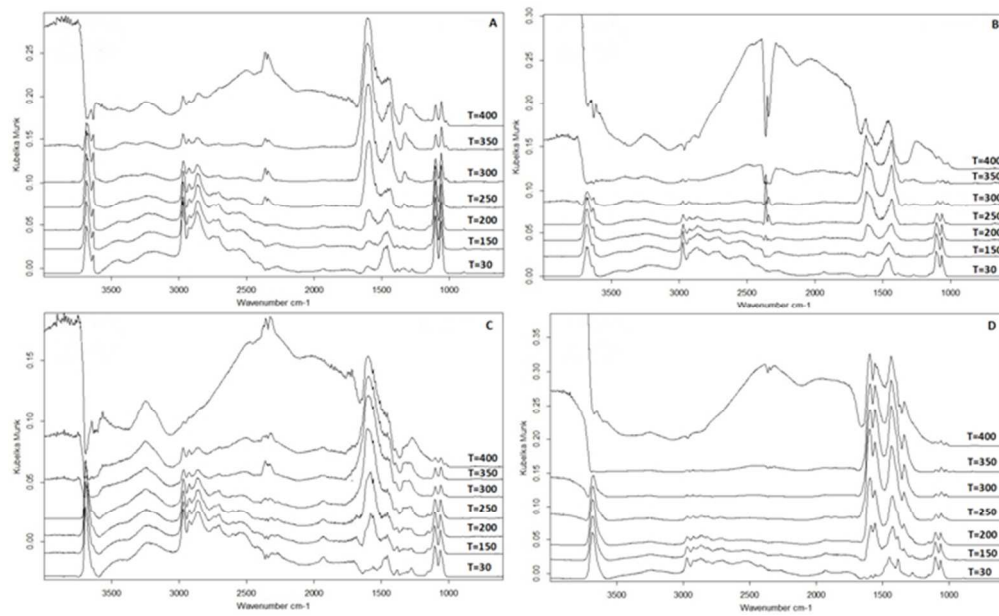


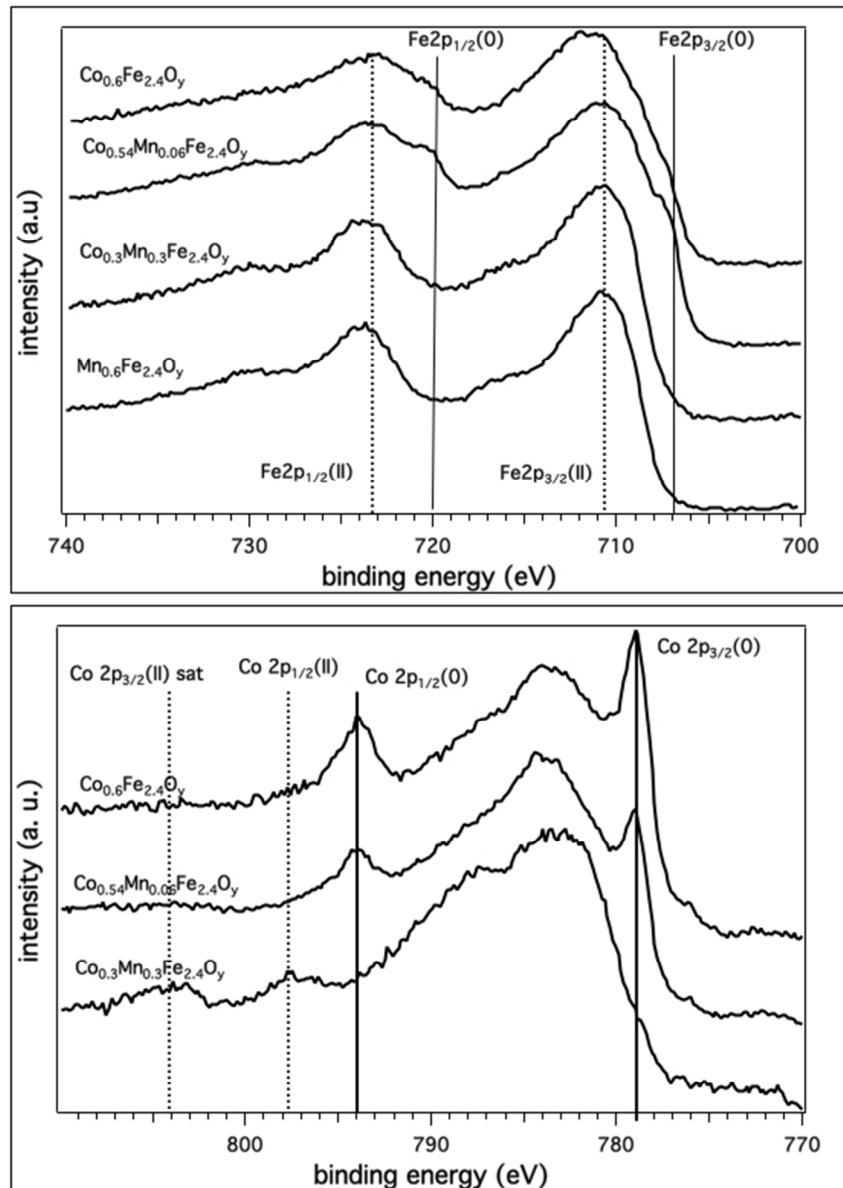


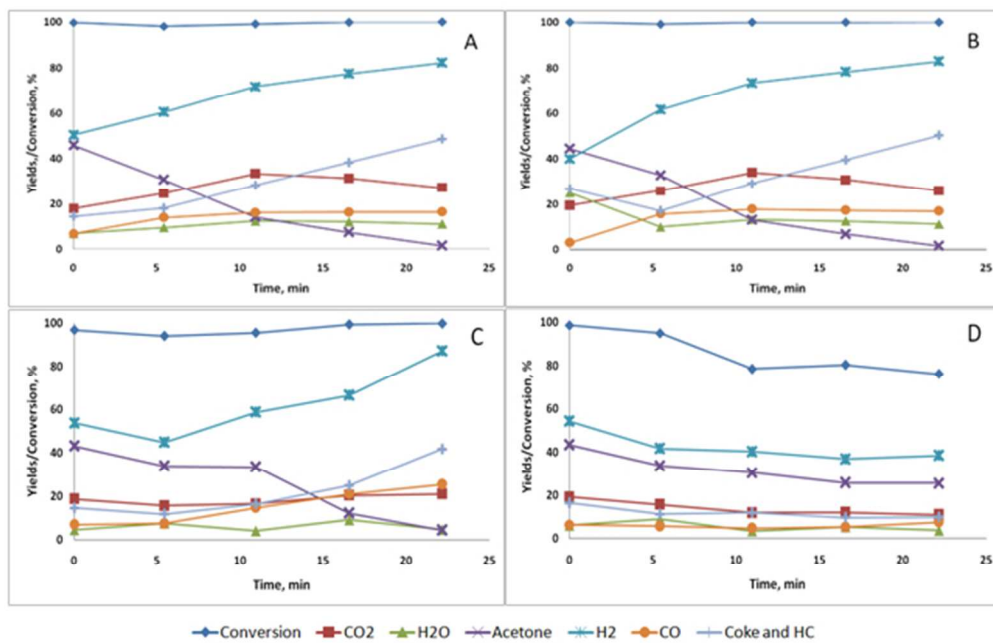


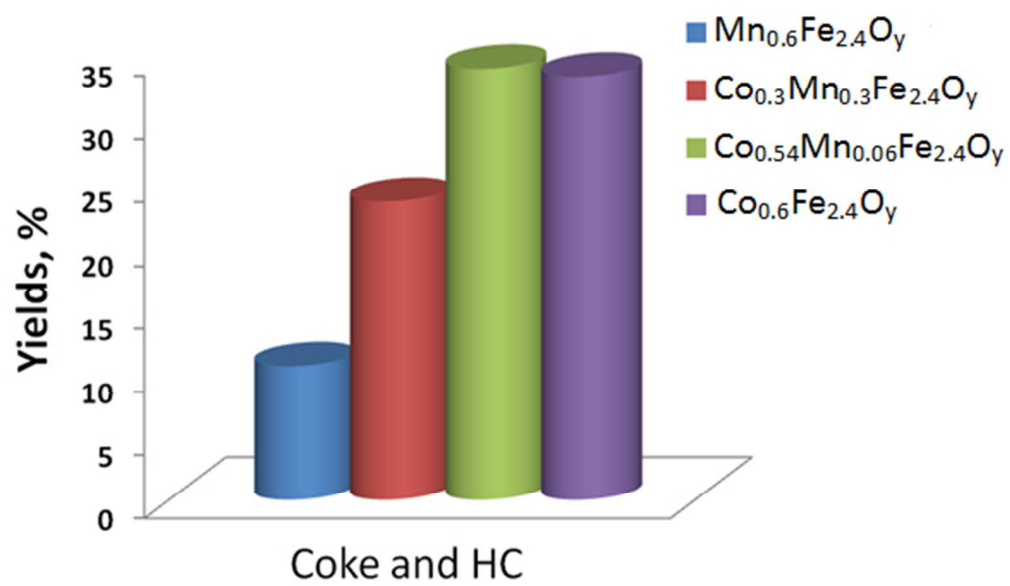


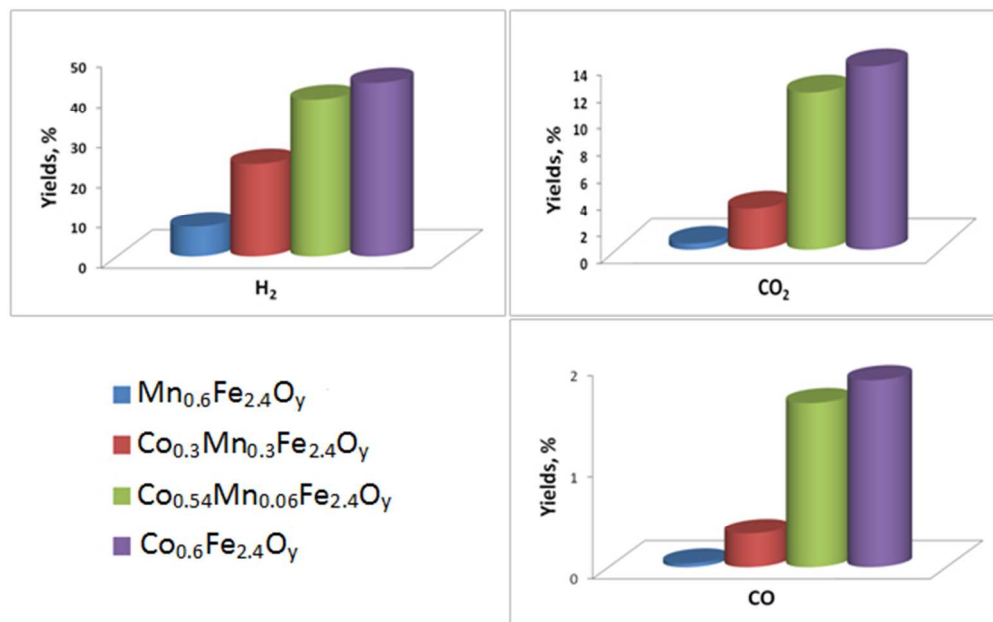


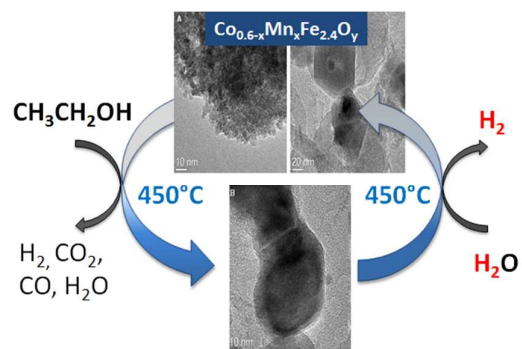












Ferrospinels of general composition  $\text{Co}_{0.6-x}\text{Mn}_x\text{Fe}_{2.4}\text{O}_y$  were studied as  $\text{O}^{2-}$  and electrons vectors for the chemical-loop reforming of ethanol aimed at the production of clean  $\text{H}_2$ .